THE JOURNAL OF PHYSICAL CHEMISTRY A

Article

pubs.acs.org/JPCA

Electron Paramagnetic Resonance Line Shifts and Line Shape Changes Due to Heisenberg Spin Exchange and Dipole−Dipole Interactions of Nitroxide Free Radicals in Liquids 8. Further Experimental and Theoretical Efforts to Separate the Effects of the Two Interactions

Mirna Peric,*[,†,‡] Barney L. Bales,[†] and Miroslav Peric[†]

[†]Department of Physics and Astronomy and The Center for Supramolecular Studies, California State University at Northridge, Northridge, California 91330, United States

[‡]Keck School of Medicine, University of Southern California, Los Angeles, California 90089, United States

Supporting Information

ABSTRACT: The work in part 6 of this series (*J. Phys. Chem. A* **2009**, *113*, 4930), addressing the task of separating the effects of Heisenberg spin exchange (HSE) and dipole−dipole interactions (DD) on electron paramagnetic resonance (EPR) spectra of nitroxide spin probes in solution, is extended experimentally and theoretically. Comprehensive measurements of perdeuterated 2,2,6,6-tetramethyl-4-oxopiperidine-1-oxyl (pDT) in squalane, a viscous alkane, paying special attention to lower temperatures and lower concentrations, were carried out in an attempt to focus on DD, the lesser understood of the two interactions. Theoretically, the analysis has been extended to include the recent comprehensive treatment by Salikhov (*Appl. Magn. Reson.* **2010**, *38*, 237). In dilute solutions, both interactions (1) introduce a dispersion component, (2) broaden the lines, and (3) shift the lines. DD introduces a dispersion component proportional to the concentration and of opposite sign to that of HSE. Equations relating the EPR spectral parameters to the rate constants due to HSE and DD have been derived. By employing nonlinear least-squares fitting of theoretical spectra to a simple analytical function and the proposed equations, the contributions of the two interactions to items 1−3 may be quantified and compared with the same parameters obtained by fitting experimental spectra. This comparison supports the theory in its broad predictions; however, at low temperatures, the DD contribution to the experimental dispersion amplitude does not increase linearly with concentration. We are unable to deduce whether this discrepancy is due to inadequate analysis of the experimental data or an incomplete theory. A new key aspect of the more comprehensive theory is that there is enough information in the experimental spectra to find items 1−3 due to both interactions; however, in principle, appeal must be made to a model of molecular diffusion to separate the two. The permanent diffusion model is used to illustrate the separation in this work. In practice, because the effects of DD are dominated by HSE, negligible error is incurred by using the model-independent extreme DD limit of the spectral density functions, which means that DD and HSE may be separated without appealing to a particular model.

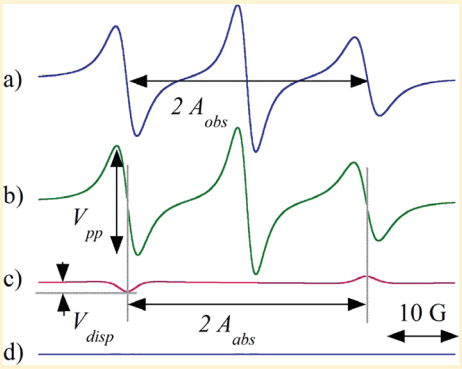

INTRODUCTION

To realize the full potential of nitroxide spin probes (nitroxides) to study molecular motion in liquids, the effects of Heisenberg spin exchange (HSE) and dipole−dipole interactions (DD) must be separated. (See Table 1 for a list of frequently used acronyms and abbreviations.) This fact has been recognized for many years,[1] but a successful experimental approach to effect the separation has only recently been proposed in part 6[2] of this series on line shape changes of the electron paramagnetic resonance (EPR) spectra of nitroxides. Independently, over about the same time span, theoretical progress was being made by Salikhov and co-workers[3,4] who, taking into account all coherence transfer processes, treated the effects of DD more comprehensively than the standard motional narrowing treatments.[5]

HSE and DD produce rather complex changes in EPR spectra, broadening and shifting the lines while introducing a dispersion component. In part 6,[2] we used the amplitude of the dispersion component to measure the rate constant of HSE, K_{ex}, and the line width to independently measure the rate constant of line broadening, K_B. From these quantities we were able to deduce the rate constant of DD broadening, K_{dip}. The

Received: October 19, 2011
Revised: January 27, 2012
Published: January 30, 2012

Table 1. Abbreviations and Acronyms

DD	dipole−dipole interactions
HSE	Heisenberg spin exchange
instrumental dispersion	in-phase magnetization, commonly due to an improperly balanced microwave bridge
dispersion	HSE or DD induced dispersion corrected for instrumental dispersion
negative dispersion	$\pm V_{disp}(\pm) < 0$ for a spectrum where the doubly integrated intensity is positive
FIT	linear or nonlinear least-squares fit (noun)
FITTING	linear or nonlinear least-squares fitting (verb)
PDM	permanent diffusion model
SE	Stokes−Einstein model
SES	Stokes−Einstein−Smoluchowski equation
70%AG	70 wt % glycerol in water

separation of HSE and DD relied on an assumption that DD did not contribute to the dispersion component.[5]

At low values of T/η, where η is the shear viscosity, we found a curious phenomenon: the dispersion was of opposite sign to that produced by HSE. The recent theory predicts a negative dispersion when DD dominates, so we speculated that the new theory might apply but did not attempt a quantitative analysis because the results for nitroxides were not available at that time. Sailkohv's recent work[4] applied the new theory to the cases of ^{14}N and ^{15}N nitroxides, encouraging us to attempt such an analysis. Two complications arose: (1) the nonlinear least-squares fits (FITS) from which the dispersion components are deduced showed small, but definite residuals, so we could not be sure that the negative dispersions were not artifacts, and (2) the negative dispersion only increased with concentration (c, in mol L^{-1}) up to a critical concentration, above which it became constant.[2]

The spectral lines of the time-resolved EPR spectra of spin-correlated micelle-confined radical pairs are split into pairs of lines of opposite phases.[6−9] These so-called anti-phase structures (APS) are also produced by HSE and DD between two radicals forming a radical pair. The broadening and line shifts of APS lines as well as the change of APS sign[7,8] are in many ways similar to the spectral EPR line changes observed in the present work.

The present work was undertaken with two main purposes in mind: (1) to reframe Salikhov's theory in terms of parameters usually measured in the laboratory that are available from FITS and (2) to carry out another careful experiment in a viscous liquid to complement our previous work[2] in 70%AG. We chose to study perdeuterated 2,2,6,6-tetramethyl-4-oxopiperidine-1-oxyl (pDT) in the viscous alkane, squalane, in order to emphasize low values of T/η where DD is expected to dominate, paying special attention to the low-c region to further investigate the peculiar concentration dependence of the dispersion. The choice of squalane affords the opportunity to study pDT in a pure solvent of molecules considerably larger than the spin probe.

Some of the complexity of Salikhov's[4] treatment stems from different behaviors of the line shape when $(J_0\tau_c)^2 > 1$ (strong HSE) as opposed to the opposite limit (weak HSE), where J_0 is the exchange integral and τ_c is the mean duration of the collision. We restrict our discussion to strong HSE because it invariably has been shown to apply to uncharged nitroxides except in very low viscosity solvents.[10]

THEORY

In the case of ^{14}N nitroxide spin probes, all spins in a solution can be divided into three subensembles having projections +1, 0, and −1 of the nitrogen nuclear spin. The motion of the transverse components of the subensemble magnetization vectors $M_1^\perp$, $M_0^\perp$ and $M_{-1}^\perp$ is described by the modified Bloch equations[3,4,11,12]

$$\begin{aligned}
\frac{\partial M_1^\perp}{\partial t} &= -i(\omega_0 - a_0 + b_{ER}n - \omega)M_1^\perp - \frac{1}{T_{12}}M_1^\perp \\
&\quad + WnM_1^\perp + VnM_0^\perp + VnM_{-1}^\perp - i\omega_1 M_0 \\
\frac{\partial M_0^\perp}{\partial t} &= -i(\omega_0 - \omega)M_0^\perp - \frac{1}{T_{02}}M_0^\perp + WnM_0^\perp + VnM_1^\perp \\
&\quad + VnM_{-1}^\perp - i\omega_1 M_0 \\
\frac{\partial M_{-1}^\perp}{\partial t} &= -i(\omega_0 + a_0 - b_{ER}n - \omega)M_{-1}^\perp - \frac{1}{T_{-12}}M_{-1}^\perp \\
&\quad + WnM_{-1}^\perp + VnM_0^\perp + VnM_1^\perp - i\omega_1 M_0
\end{aligned} \tag{1}$$

where $M_j^\perp = M_{jx}^\perp - iM_{jy}^\perp$, $j = -1$, 0, and 1, n is the number of spins per unit volume, $\omega_0 = g\beta H_0/\hbar$ is the Zeeman frequency of the spin probe in the external magnetic field H_0, g is the radical g-factor, β is the Bohr magneton, $\hbar$ is the Planck constant, $\omega_1 = g\beta H_1/\hbar$ is the nutation frequency corresponding to a nonsaturating microwave field H_1, ω is the angular frequency corresponding to the sweeping microwave field, a_0 is the hyperfine coupling constant in rad/s ($a_0 = g\beta A_0/\hbar$, where A_0 is the hyperfine coupling spacing in Gauss), and M_0 is the longitudinal component of the subensemble equilibrium magnetization vector. T_{12}, T_{02}, and T_{-12} are the transverse relaxation times of the three subensembles in the absence of DD and HSE, that is, the reciprocals of the intrinsic unsaturated line widths. The term b_{ER} accounts for spin precession and re-encounters during the collision encounter[12,13]

$$b_{ER} = \pm\frac{1}{2}K_{ex}\left[\gamma A_0\tau_C + \frac{1}{3}(1+\sqrt{2})\sqrt{\gamma A_0\tau_{RE}/2}\right] \tag{2}$$

where τ_{RE} is the time interval between re-encounters. Salikhov[4] showed that the outer lines shift away from the center for weak HSE (plus sign) and toward the center for strong HSE (minus sign). Despite many claims in the literature that a transition from strong to weak HSE was observed, the only convincing case was given by Plachy and Kivelson[10] who appealed to the Stokes−Einstein (SE) equation. Still under discussion is the strength of HSE for Fremy's salt.[11,14−16] All of the previous work relied on line-width measurements and required a comparison of the experimental results with a model of molecular diffusion (usually the SE) at varying values of T/η. Perhaps careful studies of line shifts could provide an additional criterion for the strength of HSE.

The terms containing W and V in eqs 1 describe the loss of the spin coherence (W) and the spin coherence transfer (V)

induced by HSE and DD between spin probes.[4] The dephasing rate constant W is given by[4]

$$W = W_{ex} + W_{dd} = \frac{2K_{ex}}{3} + \alpha^2\left[\frac{3}{8}J^{(2)}(2\omega_0) + \frac{11}{4}J^{(1)}(\omega_0) + \frac{19}{72}J^{(0)}(0)\right] \quad (3)$$

where W_{ex} describes the contribution from HSE, W_{dd} from DD, $\alpha^2 = S(S+1)g^4\beta^4/\hbar^2$, and $J^{(n)}(\omega)$ are spectral densities of the correlation functions for DD.[5] The spin coherence transfer rate constant V is given by[4]

$$V = V_{ex} + V_{dd} = \frac{K_{ex}}{3} - \frac{1}{3}\alpha^2\left[\frac{3}{2}J^{(1)}(\omega_0) + \frac{1}{6}J^{(0)}(0)\right] \quad (4)$$

where V_{ex} and V_{dd} describe the contributions from HSE and DD, respectively. The spectral densities depend on the kinematics of the molecular motion. If we assume that the molecular diffusion is described by the so-called permanent diffusion model (PDM), the spectral densities can then be calculated in terms of the translational diffusion time, τ_D, as described in Section 3 of ref 4. As can be noted from eq 4, the contribution from DD to the spin coherence transfer is opposite that from HSE: negative for DD, and positive for HSE. The contributions of both interactions to W are positive (eq 3).

We note that

$$V_{dd} = -bW_{dd} \quad (5)$$

$$V_{ex} = W_{ex}/2 \quad (6)$$

where

$$b = \frac{\frac{1}{3}\left[\frac{3}{2}J^{(1)}(\omega_0) + \frac{1}{6}J^{(0)}(0)\right]}{\frac{3}{8}J^{(2)}(2\omega_0) + \frac{11}{4}J^{(1)}(\omega_0) + \frac{19}{72}J^{(0)}(0)} \quad (7)$$

In principle, b depends on the details of the molecular diffusion, that is, τ_D; however, we demonstrate below, using the PDM, that a negligible error results in the separation of DD and HSE for a typical nitroxide by taking it to be constant, $b = 1/4.75$. As the rate of diffusion decreases, τ_D increases, that is, $\omega_0\tau_D > 1$, which makes $J^{(2)}(2\omega_0) = J^{(1)}(\omega_0) \rightarrow 0$.[5] Thus eq 7 becomes $b \rightarrow 1/3[(1/6)J^{(0)}(0)]/[(19/72)J^{(0)}(0)] = 1/4.75$.

The EPR spectrum is described by the quantity

$$S(\omega) \propto -\mathrm{Im}(M_1^{\perp}(\omega) + M_0^{\perp}(\omega) + M_{-1}^{\perp}(\omega)) \quad (8)$$

The simulated spectra in this paper are computed by Mathcad at the X-band for various values of τ_D using the PDM with the following parameters: closest distance between the two colliding radicals $r_0 = 0.7$ nm,[17] twice the van der Waals radius of pDT, and the exchange integral $J(r) = J(r_0)\exp(-\lambda[r - r_0])$ with $\lambda = 20$ nm^{-1}, $J(r_0) = 10^{11}$ rad/s[4] and the X-band frequency $\omega = 6 \times 10^{10}$ rad/s. The first-derivative EPR spectra, $dS(\omega)/d\omega$, as a function of the rate of DD in the absence of HSE and vice versa are presented in the Supporting Information.

The content of eqs 1 may be encapsulated in measurable quantities in the following simple analytical form:

$$Y'(H) = \sum_{M_j}(V_{pp}(M_j)S_{M_j}(H) + V_{disp}(M_j)D_{M_j}(H)) \quad (9)$$

which is a sum of first-derivative absorption, $S_{M_j}(H)$, and dispersion, $D_{M_j}(H)$, EPR lines,[13,17−19] where H is the swept magnetic field. $D_{M_j}(H)$ is an HSE- and/or DD-induced "dispersion." The sum in eq 9 is over the nuclear quantum numbers $M_j = +1$, 0, and −1. $S_{M_j}(H)$ is a Lorentzian−Gaussian sum function, which is a good approximation to the Voigt line shape given by eq 5 of ref 20. The spectrum, eq 9, is defined by the resonance fields of the lines, H_{M_j}, the peak-to-peak line widths including inhomogeneous broadening by unresolved hyperfine structure and field modulation and so forth, ΔH^0_{pp}, mixing parameters from which the separate Lorentzian, ΔH^L_{pp}, and Gaussian, ΔH^G_{pp}, contributions to ΔH^0_{pp} may be computed, the peak-to-peak amplitudes of the absorption components, $V_{pp}(M_j)$, and the maximum (minimum) values of the dispersion components $V_{disp}(M_j)$. The expression for $D_{M_j}(H)$ is given by eq 10 of ref 18. Note that for the "normal" presentation in which the doubly integrated spectrum is positive, $M_jV_{disp}(M_j) > 0$ for HSE and $M_jV_{disp}(M_j) < 0$ for DD. For small HSE and DD, Salikhov[3,4] has shown that eq 9 is valid. In the case of HSE, we previously showed that eq 9 holds even for large values of $K_{ex}c \approx \gamma A_0$ where the three lines begin to coalesce.[18]

To illustrate the DD case, Figure 1a shows a spectrum simulated using eqs 1 and 4 in the absence of HSE. The FIT of the spectrum to eq 9 is indistinguishable from the spectrum. The difference in the spectrum and the FIT is given in Figure 1d showing that the FIT is excellent. Figures 1b and 1c separately show the three absorption lines and the two "dispersion" lines, respectively. The measured amplitudes and

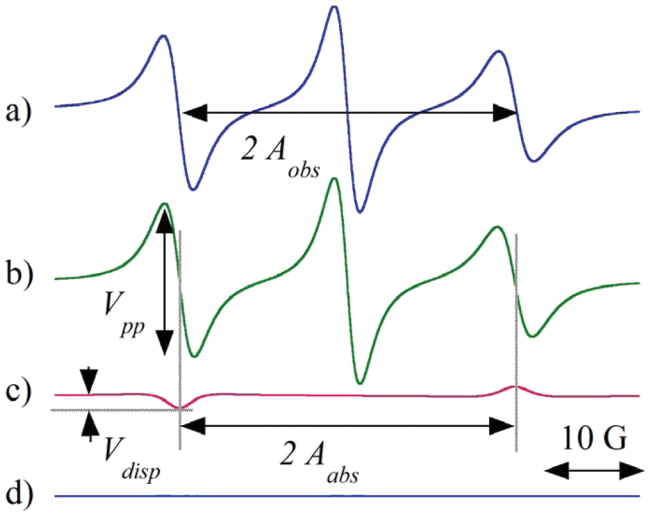

Figure 1. (a) Simulated DD (zero HSE) EPR spectrum having $1/\gamma T_{12} = 0.45$ G, $1/\gamma T_{02} = 0.3$ G, $1/\gamma T_{-12} = 0.8$ G, $A_0 = 14.4$ G, $W_{dd}/\gamma = 80$ G/M, $V_{dd}/\gamma = 16.8$ G/M, and $c = 0.015$ M calculated using eqs 1. Note that V^{dip}_{disp} is negative for the low field line, $M_j = +1$, which is the opposite of that found for HSE. The difference of the simulated spectrum (a) and the sum of the three absorption lines (b) and the two dispersion lines (c) is a straight line (d), indicating an excellent fit.

dx.doi.org/10.1021/jp210057x | J. Phys. Chem. A 2012, 116, 2855−2866

line spacings are defined in Figure 1. Note that V^{dip}_{disp} is negative for the low field line, $M_j = +1$, while V^{ex}_{disp} is positive. The peak-to-peak broadening for a given line M_j is given by the following:

$$B(M_j) = \Delta H^{L}_{pp}(c)_{M_j} - \Delta H^{L}_{pp}(0)_{M_j} = B_{ex}(M_j) + B_{dip}(M_j) \quad (10)$$

where $\Delta H^{L}_{pp}(c)_{M_j}$ is the Lorentzian line width at concentration c broadened by HSE and/or DD, and $\Delta H^{L}_{pp}(0)_{M_j}$ is the Lorentzian line width in the absence of these interactions. It is worth reemphasizing that $B_{ex}(M_j)$ and $B_{dip}(M_j)$ must be computed from the Lorentzian component of the line width, not the overall line width; using ΔH^{0}_{pp} in eq 10 introduces errors that are not severe in the case of pDT but can be considerable for other spin probes.[20] Further note that $\Delta H^{L}_{pp}(c)_{M_j}$ is the line width of the absorption component of each line separately, taking into account overlap with other absorption lines and dispersion components. The parameters of each line separately may be found easily by FITTING. Salikhov[4] gives expressions for the line widths and amplitudes of the dispersion components of the spectrum in the limit of small c, not taking into account line overlap.

For small Wc and Vc, the peak-to-peak quantities are related to the rate constants in eqs 1 by the following (see the Supporting Information):

$$B_{ex}(M_j) = \frac{2}{3}\frac{2}{\gamma\sqrt{3}}K_{ex}c \quad (11)$$

$$B_{dip}(M_j) = \frac{2}{\gamma\sqrt{3}}W_{dd}c \quad (12)$$

$$A_0 M_j\left(\frac{V^{ex}_{disp}(M_j)}{V_{pp}(M_j)}\right) = \frac{2}{3}\frac{2}{\gamma\sqrt{3}}K_{ex}c \quad (13)$$

$$A_0 M_j\left(\frac{V^{dip}_{disp}(M_j)}{V_{pp}(M_j)}\right) = 2\frac{2}{\gamma\sqrt{3}}V_{dd}c \quad (14)$$

where $V_{disp}(M_j) = V^{dip}_{disp}(M_j) + V^{ex}_{disp}(M_j)$. For the central line, $V^{ex}_{disp}(0) = V^{dip}_{disp}(0) = 0$. Due to the fact that the experimental fitting provides the total broadening B and $V_{disp}(M_j)$, which contain the contributions from both HSE and DD, we need to use the procedure proposed below to separate these contributions.

For increasing values of $K_{ex}c$, eqs 1 show that the outer lines broaden faster than the central line, and the dependence of $V_{disp}(M_j)/V_{pp}(M_j)$ becomes nonlinear; nevertheless, eqs 11−14 are still valid provided that $B_{ex}(M_j)$ is replaced by its average over three lines, $\langle B_{ex}\rangle$ and that $V_{disp}(M_j)/V_{pp}(M_j)$ is corrected so that $(V^{ex}_{disp}/V_{pp})^{\#} = B_{ex}/A_0$ as described in the Supporting Information.

A plot of $(V_{disp}/V_{pp})^{\#}$ versus $\langle B\rangle/A_0$ is expected to yield a straight line passing through the origin because both are proportional to c. Let the slope of this line be denoted by k.

$$\left(\frac{V_{disp}}{V_{pp}}\right)^{\#} = k\frac{\langle B\rangle}{A_0} \quad (15)$$

In terms of the parameters of eqs 1, we may show using eqs 11−14 employing eq 5 that

$$k = \frac{\frac{2}{3}K_{ex} - 2bW_{dd}}{\frac{2}{3}K_{ex} + W_{dd}} \quad (16)$$

Equation 15, in the extremes of DD and HSE, becomes

$$\left(\frac{V^{dip}_{disp}}{V_{pp}}\right) = -2b\frac{\langle B_{dip}\rangle}{A_0} \text{ and } \left(\frac{V^{ex}_{disp}}{V_{pp}}\right)^{\#} = \frac{\langle B_{ex}\rangle}{A_0} \quad (17)$$

Define the ratio of the broadening by HSE to the broadening, Ω, as follows:

$$\Omega = \frac{\langle B_{ex}\rangle}{\langle B\rangle} = \frac{\frac{2}{3}K_{ex}}{\frac{2}{3}K_{ex} + W_{dd}} \quad (18)$$

Thus,

$$\langle B_{ex}\rangle = \Omega\langle B\rangle \quad (19)$$

and from eq 10

$$\langle B_{dip}\rangle = (1 - \Omega)\langle B\rangle \quad (20)$$

Equation 15 may be rewritten as

$$\left(\frac{V^{ex}_{disp}}{V_{pp}}\right)^{\#} + \left(\frac{V^{dip}_{disp}}{V_{pp}}\right) = k\frac{\langle B\rangle}{A_0} \quad (21)$$

which becomes, combining eqs 5, 6, and 11−14,

$$\frac{\langle B_{ex}\rangle}{A_0} - 2b\frac{\langle B_{dip}\rangle}{A_0} = k\frac{\langle B\rangle}{A_0} \quad (22)$$

or

$$\frac{\langle B\rangle\Omega}{A_0} - 2b\frac{\langle B\rangle(1 - \Omega)}{A_0} = k\frac{\langle B\rangle}{A_0} \quad (23)$$

from which a simple formula to compute Ω emerges as follows:

$$\Omega = \frac{k + 2b}{1 + 2b} \quad (24)$$

Coherence transfer by both DD and HSE affects the positions of EPR lines. There are two shifts.[16,18] One shifts the resonance frequency of the outer absorption EPR lines, resulting in a hyperfine spacing, A_{abs}, that is defined to be one-half of the difference in the resonance fields of the high- and low-field absorption lines. Note that one-half the difference in the maxima and minima of the dispersion lines is also A_{abs}, where abs refers to the absorption lines. If significant line overlap occurs, A_{abs} must be found from the separation of the individual lines. The second shift is due to overlap of the dispersion lines pushing the outer lines either farther toward the center ($(V_{disp}/V_{pp})^{\#} > 0$) or away from it ($(V_{disp}/V_{pp})^{\#} < 0$). This results in a hyperfine spacing, A_{obs}, defined as one-half the difference in the fields where the low- and high-field lines cross the baseline (Figure 1a). The observed spacing A_{obs} can be directly measured from the EPR spectrum when it is defined, while A_{abs} can be found in general only by spectral fitting.

dx.doi.org/10.1021/jp210057x | J. Phys. Chem. A 2012, 116, 2855−2866

Table 2. Input Values to Compute Eqs 1[a]

τ_D, ns	K_{ex}/γ, G	W_{dd}/γ, G	$-V_{dd}/\gamma$, G	$1/b = -W_{dd}/V_{dd}$	k[b]	Ω[c]
	338[d]	0	0		1.00	1.00
0.10	338	0.731	0.144	5.09	0.995	0.997
0.50	76.3	2.92	0.610	4.79	0.923	0.946
1.0	40.0	5.73	1.20	4.76	0.749	0.823
1.5	27.4	8.54	1.80	4.76	0.547	0.681
2.0	20.9	11.4	2.39	4.76	0.362	0.551
2.5	17.0	14.2	2.98	4.75	0.209	0.443
3.0	14.3	17.0	3.58	4.75	0.0891	0.359
3.5	12.4	19.8	4.18	4.75	−0.00396	0.293
4.0	10.9	22.7	4.77	4.75	−0.0753	0.243
4.5	9.76	25.5	5.37	4.75	−0.132	0.203
5.0	8.84	28.3	5.96	4.75	−0.176	0.172
		28.3[e]	5.96	4.75	−0.421	0.00

[a] A_0 = 14.4 G, $\Delta H^L_{pp}(0) = 2(0.5/\sqrt{3})$ G for all three lines, and $\kappa_{ER} = 0.0823$. [b] Slope (eq 15) computed from the PDM: $k = (2K_{ex}/3 + 2V_{dd})/(2K_{ex}/3 + W_{dd}) = (2K_{ex}/3 - 2bW_{dd})/(2K_{ex}/3 + W_{dd})$. The slope computed using a fixed $b = 1/4.75$ is the same within 2×10^{-4}. [c] Equation 24. [d] Pure HSE. [e] Pure DD.

The resonant field shift is given by eq 2.83 of Molin et al.[11,16] as

$$H(B)_{M_j} - H(0)_{M_j} = \phi_{M_I}\left(\frac{3\sqrt{3}}{4} M_j A_0 \frac{V_{disp}(M_j)}{V_{pp}(M_j)}\right)^2 \sum_{M'_j \neq M_j} \frac{\phi_{M'j}}{H(0)_{M'j} - H(0)_{M_j}} \quad (25)$$

where the sum is over the two nuclear quantum numbers other than M_j, and ϕ_{M_j} is the statistical weight of the spins in this configuration; $\phi_{M_j} = 1/3$ for ^{14}N nitroxides. After evaluating eq 25 and assuming $A_{abs} = [H(B)_{+1} - H(B)_{-1}]/2$, we get

$$\frac{A_{abs}}{A_0} = 1 - \frac{9}{32}\left[\left(\frac{V_{disp}}{V_{pp}}\right)^{\#}\right]^2 \quad (26)$$

Finally in terms of the broadening using eq 15, we get

$$\frac{A_{abs}}{A_0} = 1 - \frac{9}{32}\left(\frac{k\langle B\rangle}{A_0}\right)^2 \quad (27)$$

Including spin precession and/or re-encounters during a collision encounter adds a linear term[4,13] to eq 27:

$$\frac{A_{abs}}{A_0} = 1 - \kappa_{ER}\Omega\frac{\langle B\rangle}{A_0} - \frac{9}{32}\left(\frac{k\langle B\rangle}{A_0}\right)^2 \quad (28)$$

where

$$\kappa_{ER} = \frac{3\sqrt{3}}{4K_{ex}} b_{ER} \quad (29)$$

The overlapping dispersion component of width $\langle B\rangle$ and amplitude $(V_{disp}/V_{pp})^{\#}$ further shifts the outer lines as developed on pp 46 and 47 of ref 11 and applied to first-derivative spectra leading to eq 24 of ref 16. The additional shifts of the $M_j = \pm 1$ lines, valid for small values of $(V_{disp}/V_{pp})^{\#}$, give the second term in the following:

$$\frac{A_{obs}}{A_0} = 1 - \frac{9}{16}\left[\frac{\Delta H^L_{pp}(0)_{\pm}}{A_0} + \frac{\langle B\rangle}{A_0}\right]\left(\frac{V_{disp}}{V_{pp}}\right)^{\#} - \kappa_{ER}\Omega\frac{\langle B\rangle}{A_0} - \frac{9}{32}\left(k\frac{\langle B\rangle}{A_0}\right)^2 \quad (30)$$

where $\Delta H^L_{pp}(0)_{\pm} = [\Delta H^L_{pp}(0)_{+} + \Delta H^L_{pp}(0)_{-}]/2$. Note that the second term shifts the lines apart when $(V_{disp}/V_{pp})^{\#} < 0$, and the third term shifts them one way or the other depending on the strength of the HSE.[4]

PREDICTIONS OF EQS 1

We now study the predictions of eqs 1 by simulating spectra with known mixtures of HSE and DD. By FITTING the simulated spectra to eq 9, we may ascertain to what extent the output parameters of the FITS yield correct values of the input parameters. The input parameters for HSE and DD computed from the PDM are given in Table 2. Note that the values of $1/b$ computed from eq 7 (column 5) quickly converge to the slow diffusion limit of 4.75 at rather fast diffusion rates. Columns 6 and 7 give the values of k and Ω, computed from eqs 16 and 18, respectively. To replicate a typical experiment, spectra were simulated at a series of values of concentrations up to values of $\langle B\rangle/A_0 \approx 0.25$.

There is a negligible difference in values of $\langle B\rangle/A_0$ computed from the input values and the results of FITTING the spectra to eq 9. Values of $(V_{disp}/V_{pp})^{\#}$ and A_{abs}/A_0 derived from the FITS are plotted as functions of $\langle B\rangle/A_0$ in Figures 2 and 3, respectively. The slopes of the straight lines in Figure 2 yielded the FITTED values of k given in column 2 of Table 3, which may be compared with the input values in Table 2. Errors in the values of k derived from FITTING near $k = 0$ are large as expected, but the maximum error in the parameter of importance, Ω, is $[((\Omega_{in} - \Omega_{out})/\Omega_{in})100] = 1.3\%$, where Ω_{in} is from Table 2 and Ω_{out} is from Table 3, and the average error is negligible. The solid lines in Figure 3 are FITS to eq 28 yielding the values of k in column 3 of Table 3 and of κ_{ER} in column 6. Values of Ω derived from the line shifts are given in column 5; these are within 1.3% of the correct (input) values.

dx.doi.org/10.1021/jp210057x | J. Phys. Chem. A 2012, 116, 2855−2866

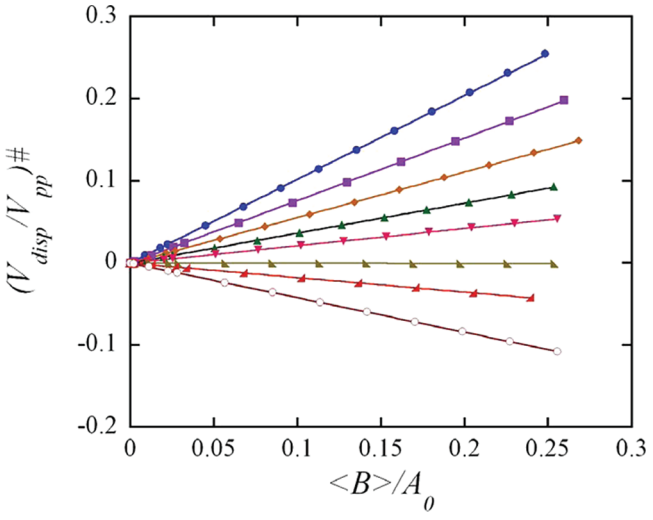

Figure 2. Dispersion−absorption height ratio versus normalized broadening due to HSE and DD for different values of the translational diffusion time τ_D simulated by eqs 1. HSE only (●); τ_D = 1.0 ns (■); τ_D = 1.5 ns (♦), τ_D = 2.0 ns (▲); τ_D = 2.5 ns (▼); τ_D = 3.5 ns (left triangle); τ_D = 5.0 ns (right triangle); and DD only (○). The lines are fits of the data to eq 15.

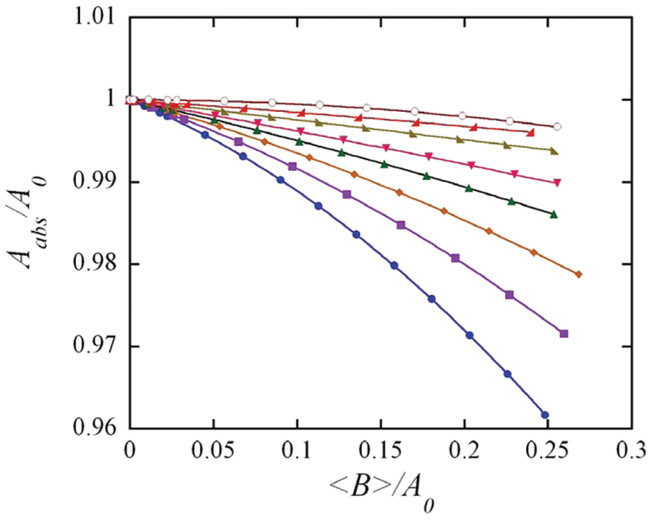

Figure 3. Normalized absorption hyperfine coupling spacing versus normalized broadening due to HSE and DD for different values of the translational diffusion time τ_D simulated by eqs 1. HSE only (●); τ_D = 1.0 ns (■); τ_D = 1.5 ns (♦), τ_D = 2.0 ns (▲); τ_D = 2.5 ns (▼); τ_D = 3.5 ns (left triangle); τ_D = 5.0 ns (right triangle);and DD only (○). The lines are fits of the data to eq 28.

Comparing the final column of Table 3 with the input value of κ_{ER} = 0.0823 shows that this parameter is recovered to within 1.7%.

In principle, Ω depends on b; however, using a fixed value of b = 1/4.75 changes Ω by only 2 × 10^{-4} for a typical nitroxide, so, in practice, the constant value may be used for computations. Thus, we conclude that FITTING faithfully reproduces the content of eqs 1. Note that $(V_{disp}/V_{pp})^{\#}$ requires correction at large values, but that A_{abs}/A_0 does not, being accurately given by the perturbation prediction, eq 28.

Values of A_{obs}/A_0 extracted from the simulated spectra are plotted versus $\langle B\rangle/A_0$ in Figure 4, while the solid lines are plots of eq 30. Thus, eq 30 is a good approximation of A_{obs}/A_0 to $\langle B\rangle/A_0 \approx 0.15$. Note that for the top two curves where DD

Table 3. Results of FITTING Simulated Spectra Using the Parameters of Table 2

τ_D, ns	k^a	k^b	Ω^a	Ω^b	κ_{ER}
0.10	1.01	1.01	1.01	1.01	0.0828
0.50	0.940	0.937	0.957	0.956	0.0837
1.0	0.762	0.761	0.833	0.832	0.0837
1.5	0.556	0.556	0.688	0.688	0.0836
2.0	0.365	0.362	0.553	0.551	0.0824
2.5	0.211	0.210	0.445	0.444	0.0826
3.0	0.0896	0.0782	0.359	0.351	0.0819
3.5	−0.004	−0.008	0.294	0.291	0.0823
4.0	−0.076	−0.081	0.243	0.239	0.0824
4.5	−0.133	−0.132	0.203	0.203	0.0821
5.0	−0.177	−0.178	0.172	0.171	0.0824

[a]Derived from $(V_{disp}/V_{pp})^{\#}$ vs $\langle B\rangle/A_0$. [b]From A_{abs}/A_0 vs $\langle B\rangle/A_0$. These values were fit using the curves in Figure 3 up to $\langle B\rangle/A_0$ = 0.15; FITTING to 0.25 introduces an additional 1% error.

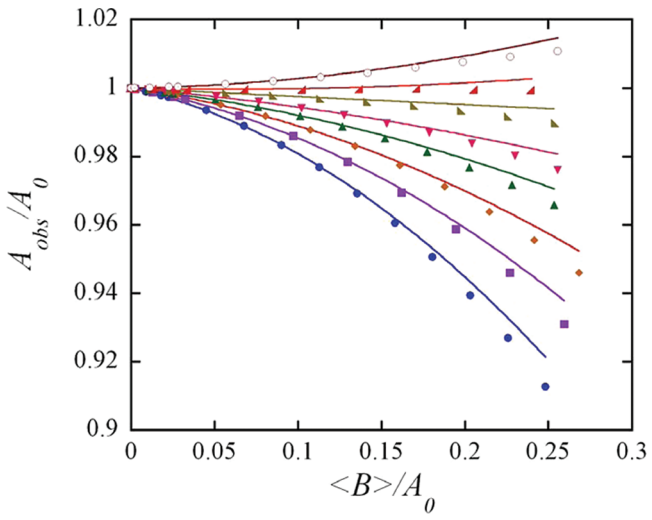

Figure 4. Normalized observed hyperfine coupling spacing versus normalized broadening due to HSE and DD for different values of the translational diffusion time τ_D simulated by eqs 1. HSE only (●); τ_D = 1.0 ns (■); τ_D = 1.5 ns (♦), τ_D = 2.0 ns (▲); τ_D = 2.5 ns (▼); τ_D = 3.5 ns (left triangle); τ_D = 5.0 ns (right triangle); and DD only (○). The lines are eq 30.

dominates, A_{obs}/A_0 increases very slightly near the origin. Equation 30 does not include the effects of line overlap, thus it is not surprising that it is only approximate at higher values of $\langle B\rangle/A_0$.

■ MATERIALS AND METHODS

Perdeuterated-tempone (pDT; CDN Isotopes, Lot# A479P1) and squalane (Acros Organics, Lot# A0210456) were used as received. The viscosity of squalane was calculated using the Vogel−Fulcher form:[21] $\eta/T = (2.3756 \times 10^{-8})\exp[1411/(T - 128.76)]$, which was obtained by fitting the literature viscosity data.[21−25] A stock solution of pDT of concentration 59.6 mM was prepared by weight in squalane. This solution was diluted to other intermediate concentrations of 57, 53, 50, 45, 40, 35, 30, 25, 20, 15, 10, 5, and 0.1 mM. The samples were drawn into a 15-cm polytetrafluoroethylene tube (PTFE; Zeus, Inc.) of 0.5 mm i.d. and 0.08/013 mm wall thickness. The tube was then folded in half, and the ends were sealed using pliers heated in an open flame.

dx.doi.org/10.1021/jp210057x | J. Phys. Chem. A 2012, 116, 2855−2866

EPR measurements were carried out with a Bruker ESR 300E spectrometer equipped with a Bruker variable-temperature unit. The PTFE tube was inserted in a standard 4 mm diameter EPR quartz tube made by Wildmad Glass Co. The quartz tube had a hole in the bottom allowing for nitrogen equilibration of the sample, which reduced the broadening of the EPR lines caused by molecular oxygen.[26,27] Each sample was equilibrated with nitrogen for at least 1 h before the first EPR scan. An Omega temperature indicator was used to measure the sample temperature, which was held stable within ±0.2 °C. The thermocouple tip was always positioned at the top of the EPR cavity, to avoid reducing the cavity quality factor. Samples were measured in a temperature range from 253 to 373 K in steps of 10 K and were equilibrated at each temperature for at least 5 min to ensure uniform temperature throughout the sample. Five first-harmonic EPR spectra were acquired at each temperature, employing a sweep time of 84 s, microwave power of 5 mW, time constant of 20.5 ms, sweep width of 60.2 G, and modulation amplitude of 0.2 G. The spectra were then transferred to a personal computer and were analyzed using the computer program Lowfit as detailed previously.[13,16,18] Lowfit carries out the FITS to eq 9.

RESULTS

The top traces of Figure 5a,b show experimental spectra of 25 mM pDT in squalane at 253 and 243 K with superimposed FITS. The residuals, the spectra minus the fits shown as the bottom traces, indicate that the difference is most likely due to the ^{13}C lines. It was demonstrated that eq 9 fits experimental EPR spectra broadened by HSE extremely well (see, for example, Figure 2 of ref 16, Figures 2, 4, and 5 of ref 18, and Figure 1 of ref 2). When the spectra are broadened by significant DD, as, for example, Figures 2 and 3 of ref 2, and here in Figure 5a,b, the FITS are also excellent, except for the ^{13}C lines. These FITS lead to a Lorentzian−Gaussian mixing parameter of unity, which means that the EPR lines are Lorentzian; thus, $\Delta H_{pp}^{G} = 0$. The middle traces show the dispersion component of eq 9. Note the small instrumental dispersion of the central line. The dispersion components of the high- and low-field lines show that $\pm V_{disp}(\pm 1) < 0$, indicating the presence of DD broadening as in Figure 1c.

At low concentration, $c = 0.1$ mM, the fraction of Lorentzian increases as the temperature decreases below 303 K and with increasing temperature above 303 K. The line shapes of all spectra whose concentrations are greater than 10 mM are Lorentzian, and the goodness of the FITS increases with increasing Ω. As we discussed in ref 2, the departures of the line shape from Lorentzian when DD broadening is present are not large; in the worst case, more than 97% of the doubly integrated intensity of the spectra is accounted for by the Lorentzian line shape.

The normalized averaged line broadening $\langle B\rangle/A_0$ versus pDT concentration in squalane at several representative temperatures is shown in Figure 6. The straight lines are linear least-squares FITS to the data for which the correlation coefficients are better than 0.999. Note that in the case where DD dominates (253 K), the broadening is about 5 times less than the HSE broadening at 373 K. This linearity demonstrates that pDT is soluble, and no aggregates are formed such as those observed in Figure 3 of part 7 of this series.[28] At lower temperatures, departure from linearity is observed together with a signal component clearly not due to the monomers. The analysis in this article is limited to the range of concentrations in which pDT is fully soluble.

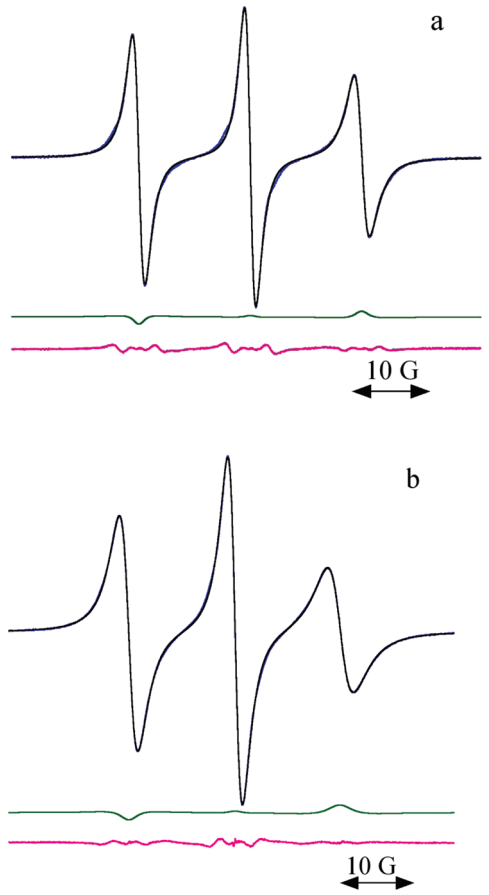

Figure 5. (a) EPR spectrum of 25 mM pDT in squalane at 253 K (top trace). The fit of the spectrum to eq 9 is indistinguishable from the spectrum, except for the wings of the lines. The spectrum minus the fit gives the residual shown as the bottom trace. It appears from the residual that the difference between the spectrum and fit comes from the ^{13}C lines. The fit gives an absorption spectrum (not shown) and a dispersion spectrum (middle trace). The central dispersion line is due to instrumental dispersion. $V_{disp}(+1) < 0$ and $V_{disp}(-1) > 0$ are due to DD. Compare with Figure 1. (b) EPR spectrum due to 25 mM pDT in squalane at 243 K (top trace). The fit is less distinguishable from the spectrum than in panel a, due to the broader lines. The dispersion (middle trace) is greater, and the residual (bottom trace) is similar to the residual in panel a, but it looks like the phase of the residual signals has changed.

Figure 7 shows the broadening rate constant, $d\langle B\rangle/dc$, as a function of T/η. A small but definite upturn can be noticed as T/η decreases toward the origin. A similar upturn has already been observed experimentally in the case of pDT in 70%AG.[2] Many authors have employed simple hydrodynamic theory to predict the behavior of the broadening rate constant as a function of T/η (see, for example, eq 9 of Berner and Kivelson[1]). Assuming that the hydrodynamic radius, the distance of closest approach, and the distance at which HSE becomes effective are equal results in the solid curved line in Figure 7, which is a poor FIT of the data. The straight line is a linear FIT to the data for $T/\eta > 20$ K/cP.

Figure 8 shows representative plots of averages of $(V_{disp}/V_{pp})^{\#}$ versus $\langle B\rangle/A_0$ for $T < 313$ K . For $T \geq 313$ K, a single straight line passing through the origin such as those predicted in Figure 2 fit the data well; however, for lower temperatures,

dx.doi.org/10.1021/jp210057x | J. Phys. Chem. A 2012, 116, 2855−2866

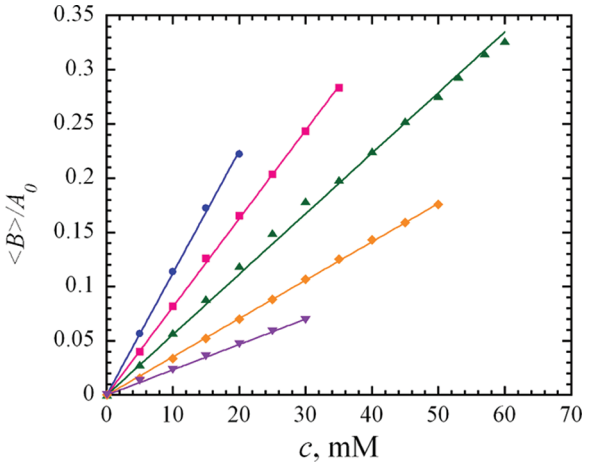

Figure 6. Normalized averaged line broadening $\langle B\rangle/A_0$ versus pDT concentration in squalane at 373 K (●), 353 K (■), 333 K (▲), 303 K (♦), and 253 K (▼). The straight lines are least-squares FITS constrained to the origin. Coefficients of correlation are better than 0.999 at all temperatures.

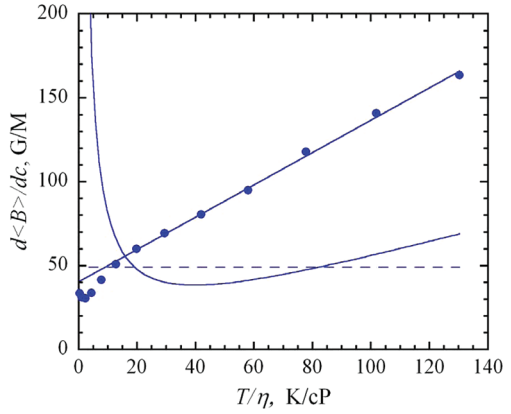

Figure 7. The broadening constant versus T/η for pDT in squalane. The uncertainties are smaller than the plot symbols. The straight line through the data is a linear least-squares FIT above T/η = 12.8 K/cP yielding $d\langle B\rangle/dc = (40.3 \pm 1.3) + (0.96 \pm 0.02)T/\eta$ in G/M with η in cP and r = 0.999. The curved line is the SE describing the sum of HSE and DD (eq 9 of ref 1). The horizontal dashed line at 49 G/M indicates the rigid limit.

the plots are not linear. The data appear to have two linear segments, a "lower" and "higher" segment. The lower segments have smaller slopes than the higher and are negative at low temperatures. The behavior at low temperatures is very similar to our previous results in 70%AG; however, here, we have collected more data at low concentrations showing that the lower segments are linear within experimental uncertainty. In our previous work,[2] we assumed that (V_{disp}^{dip}/V_{pp}) achieved a constant value in the higher segment (see Figure 7 of ref 2); thus the slope of the straight lines was equal to Ω.[2] In this work, we make the same assumption for the higher segments and compute $\Omega = k_{high}$, where k_{high} is the slope of the high segment. Figure 9 shows values of Ω. Our best attempt to quantify the uncertainties due to systematic errors represented by the error bars in Figure 9 was derived by computing Ω in two additional ways. First, we compute $\Omega = (k_{low} + 0.42)/1.42$ where k_{low} is the slope of the low segments in Figure 8; i.e., assuming that the low segments conform to eq 24. Second, we compute $\Omega = (k_{all} + 0.42)/1.42$, where k_{all} is the slope of all points in Figure

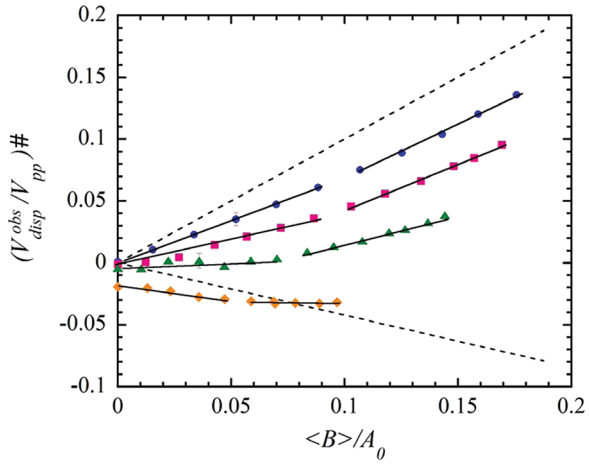

Figure 8. Values of $(V_{disp}^{obs}/V_{pp})^{\#}$ versus the total normalized broadening at 253 K (◆), 283 K (▲), 293 K (■), and 303 K (●). The straight lines are fits to two different segments of the data as explained in the text. The upper dashed line is the spin exchange limit, k = 1, and the lower dashed line is the DD limit, k = −2/4.75.

8. These represent the reasonable limits of the values of Ω. The error bars are then taken to be the standard deviation of the results of the calculations from the three approaches.

Figure 10 shows values of $d\langle B_{ex}\rangle/dc = \Omega \cdot d\langle B\rangle/dc$. The solid line is the SE prediction for any probe (eq 12 from ref 28). The measured broadening constant is greater than the hydrodynamic prediction, which should be expected since the van der Waals volume of pDT of 180 Å^3 is much less than the van der Waals volume of squalane, which is 512 Å^3.[29]

Figure 11 shows values of $d\langle B_{dip}\rangle/dc = (1 - \Omega)\cdot d\langle B\rangle/dc$ as a function η/T. The steep dashed line is the SE prediction computed from eq 13 of ref 28. As in the case of pDT in 70% AG,[2] these data quickly saturate, reaching about 35 G/M, which is less than the predicted static limit of 49.03 G.[1,2] Figure 11 is similar to Figure 10 of part 6 of this series,[2] where it was shown that the dependence was approximately logarithmic.

Plots of A_{abs}/A_0 and A_{obs}/A_0 vs $\langle B\rangle/A_0$ are similar to those for pDT in 70%AG (see Figures 11 and 12 of part 6[2]): FITS of the former, after fixing the values of Ω as described in the preceding paragraph, yield values of κ_{ER}. The discussion of re-encounter times as well as some "secondary effects" will be reported elsewhere together with results in other solvents and other probes. We note that values of A_{obs}/A_0 increase with $\langle B\rangle/A_0$ at low temperatures, similar to Figure 6 and Figure 11a of Part 6,[2] as is predicted when DD dominates.

■ DISCUSSION

At low temperature, values of $(V_{disp}^{obs}/V_{pp})^{\#}$ become negative; however, plots versus $\langle B\rangle/A_0$ are nonlinear in contradiction to the theoretical prediction, Figure 2. Previously, we attributed negative values of the dispersion to either (1) FITTING errors or (2) a true negative contribution to the dispersion introduced by DD.[2] Equations 1 provide a theoretical basis for a negative dispersion but cannot account for the nonlinear behavior in Figure 8. We interpret the results in Figure 8 using the same assumption as in Part 6:[2] the high segments become linear above a critical concentration c^* because (V_{disp}^{dip}/V_{pp}) becomes constant. To obtain the value of Ω, only the slope of the high segment is needed, so whether (V_{disp}^{dip}/V_{pp}) is derived from possibility 1 or 2 is irrelevant if we are only interested in separating HSE and DD. We have extensive data for $c < c^*$ in

dx.doi.org/10.1021/jp210057x | J. Phys. Chem. A 2012, 116, 2855−2866

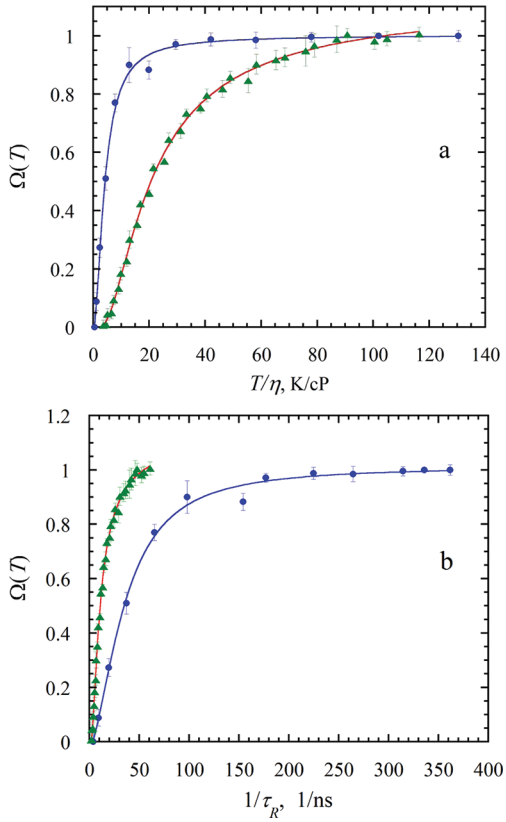

Figure 9. (a) Fractional broadening by HSE of pDT in squalane (filled circles) and 70%AG (filled triangles) versus T/η . The solid line through the pDT in squalane data is given by the empirical equation $\Omega(T) = [1.0035(T/\eta)^2 + 0.80228(T/\eta) - 0.5679]/[(T/\eta)^2 + 1.4264(T/\eta) + 17.145]$, ($r$ = 0.9986), while the solid line through the pDT in 70%AG data is given by $\Omega(T) = [1.1319(T/\eta)^2 - 6.4598(T/\eta) + 9.9385]/[(T/\eta)^2 + 5.6858(T/\eta) + 172.87]$, ($r$ = 0.9989). (b) Fractional broadening by HSE of pDT in squalane (filled circles) and 70%AG (filled triangles) versus the inverse rotational time $1/\tau_R$. The solid lines are given by $\Omega(T) = [1.0128(1/\tau_R)^2 + 15.342(1/\tau_R) - 69.863]/[(1/\tau_R)^2 + 16.483(1/\tau_R) + 1600.4]$, ($r$ = 0.9983), for pDT in squalane, and $\Omega(T) = [1.1339(1/\tau_R)^2 - 3.5073(1/\tau_R) + 2.9634]/[(1/\tau_R)^2 + 3.011(1/\tau_R) + 46.486]$, ($r$ = 0.9989), for pDT 70% AG. For pDT in squalane, DD starts at T/η = 24 K/cP when Ω = 0.95, which corresponds to η = 13.4 cP at 317 K and $1/\tau_R$ = 161 ns^{-1}, while for pDT in 70%AG, DD starts at T/η = 76 K/cP when Ω = 0.95, which corresponds to η = 4.4 cP at 337 K and $1/\tau_R$ = 40 ns^{-1}.

the present work, so we are able to pursue a more interesting question. What is the detailed behavior of $(V_{disp}^{obs}/V_{pp})^{\#}$ with concentration and temperature? We include both possibilities 1 and 2 by writing

$$(V_{disp}^{obs}/V_{pp})^{\#} = (V_{disp}^{obs}/V_{pp})_{offset} + (V_{disp}^{ex}/V_{pp})^{\#} + (V_{disp}^{dip}/V_{pp}) \quad (31)$$

Where the subscript "offset" denotes contributions due to effects other than HSE or DD.

Let us first discuss the term $(V_{disp}^{obs}/V_{pp})_{offset}$. Figure 12 shows a spectrum for c = 0.1 mM at 253 K together with the dispersion components. After correcting for the instrumental dispersion evident in the central line, we find that $(V_{disp}^{obs}/V_{pp})_+ = -0.020$ and $(V_{disp}^{obs}/V_{pp})_- = -0.023$, thus $(V_{disp}^{obs}/V_{pp}) = -0.022 \pm 0.002$. This value is within experimental uncertainty of the intercept in Figure 8. Averaging over 5 spectra, we obtain

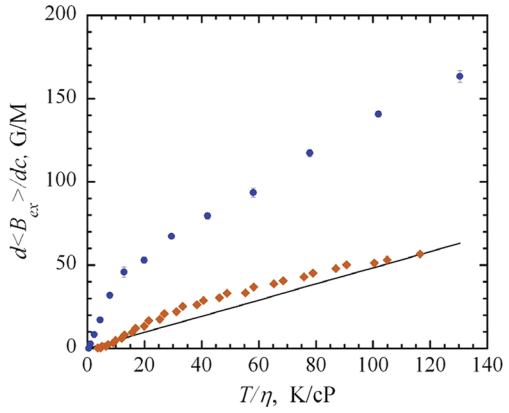

Figure 10. HSE broadening constant of pDT versus T/η in squalane (circles). The filled diamonds represent the HSE broadening constant of pDT in 70%AG.[2] The solid line is the SES prediction for pDT (eq 12 from ref 28).

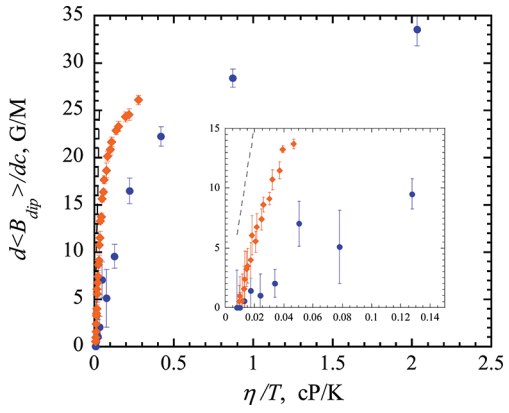

Figure 11. DD broadening constant of pDT versus η/T in squalane (circles) and 70%AG (diamonds).[2] The steep dashed line is the SE prediction for pDT (eq 13 of ref 28).

$(V_{disp}^{obs}/V_{pp})_{offset} = -0.019 \pm 0.001$ at 253 K. Similarly, we obtain values of $(V_{disp}^{obs}/V_{pp})_{offset} = -0.010$, -0.005, and -0.004 for 263,

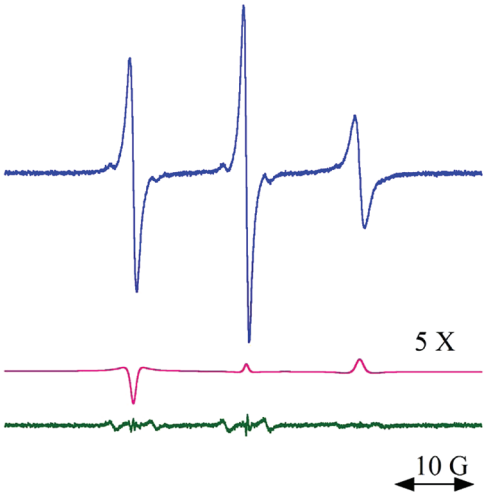

Figure 12. EPR spectrum of 0.1 mM pDT in squalane at 253 K. Note that the dispersion (5 X), shown in the middle trace, is negative. After correcting for the instrumental dispersion that is evident on the central line, the low- and high-field dispersion amplitudes are similar, $+(V_{disp}^{obs}/V_{pp})_+ = -0.020$ and $-(V_{disp}^{obs}/V_{pp})_- = -0.023$, respectively.

dx.doi.org/10.1021/jp210057x | J. Phys. Chem. A 2012, 116, 2855−2866

273, and 283 K, respectively. Above 283 K, the intercept is less than ±0.001 and is neglected. What is the source of $(V^{obs}_{disp}/V_{pp})_{offset}$? Perhaps it is due to line shape changes as the rotational motion becomes slower, although the rotational correlation time is still rather fast, $\tau_{rot} \approx 0.3$ ns. This possibility could be checked by measuring the EPR spectrum at lower microwave frequencies where rotation influences the line shape less than at X-Band. We wondered if $(V^{obs}_{disp}/V_{pp})_{offset}$ could be due to the influence of ^{13}C hyperfine lines or perhaps unresolved hyperfine structure; however, preliminary experiments with Fremy's salt in 70%AG (having neither ^{13}C lines nor unresolved hyperfine structure), show negative dispersions, similar to Figure 12. Whatever the source of $(V^{obs}_{disp}/V_{pp})_{offset}$, we assume that, at a given temperature, it is constant with c and therefore with $(\langle B\rangle/A_0)$. Thus, for $c > c^*$, differentiation of eq 31 yields

$$\begin{aligned} &d(V^{obs}_{disp}/V_{pp})^{\#}/d(\langle B\rangle/A_0) \\ &\quad = d(V^{ex}_{disp}/V_{pp})^{\#}/d(\langle B\rangle/A_0) \\ &\quad = \Omega \end{aligned} \tag{32}$$

[Note that eqs 19 and 20 in ref 2 have a typographical error, missing the term A_0]. With Ω fixed at values derived for $c > c^*$, we are then able to solve eq 31 for (V^{dip}_{disp}/V_{pp}) as follows:

$$(V^{dip}_{disp}/V_{pp}) = (V^{obs}_{disp}/V_{pp})^{\#} - (V^{obs}_{disp}/V_{pp})_{offset} - \Omega(T)\left\langle B \right\rangle/A_0 \tag{33}$$

The second term is derived from low-concentration spectra (such as Figure 12) or from the extrapolation of $(V^{obs}_{disp}/V_{pp})^{\#}$ to the origin. These are within experimental uncertainty of one another in this work.

Figure 13 shows the variation of $(V^{obs}_{disp}/V_{pp})^{\#} - (V^{obs}_{disp}/V_{pp})_{offset}$ with $\langle B\rangle/A_0$ (circles) at (a) 263 K and (b) 283 K. The solid line is $(V^{ex}_{disp}/V_{pp})^{\#} = \Omega\cdot\langle B\rangle/A_0$ using values of Ω from Figure 9. The squares are values of (V^{dip}_{disp}/V_{pp}) computed from eq 33. Values from five spectra are plotted separately to show the reproducibility and the error bars are the magnitude of one-half the difference of the values of $+(V^{obs}_{disp}/V_{pp})^{\#}_{+}$ and $-(V^{obs}_{disp}/V_{pp})^{\#}_{-}$, a measure of the systematic errors. The dashed line is the best fit of the low segments to eq 24 treating $2b$ as an adjustable parameter. If we accept the assumption that the slopes of the high segments are equal to Ω, then b is the experimental value of eq 7. The value of b derived from FITS to the low segments depend on the value of Ω. For those in Figure 9, the values of b values are tabulated in Table 4; the error bars are propagated from the errors in Ω. Meaningful values of b may only be derived from data at low temperatures. For example, we see from Table 4 that at 303 K, a 7% uncertainty in Ω leads to a 57% error in b. The experimental values of b obtained in this fashion are of the same order of magnitudes predicted by the PDM being about 50% lower at 253 K, approximately equal at 263 K, and larger above 273 K. Compare the third column of Table 4 with the fifth column of Table 2 where $2b$ varies from 0.39 to 0.41. The values of $2b$ in Table 4 increase with increasing temperature, in accord with the PDM prediction. Whether a suitable model can be devised to approximate the values in Table 4 remains to be seen.

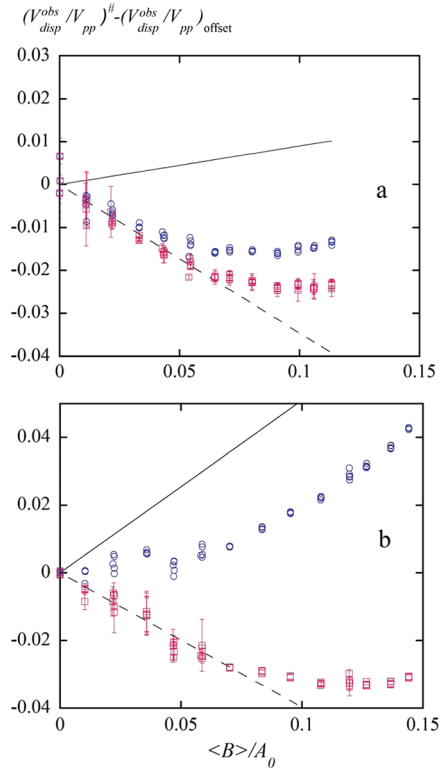

Figure 13. Values of $(V^{obs}_{disp}/V_{pp})^{\#} - (V^{obs}_{disp}/V_{pp})_{offset}$ (circles) and the DD component (squares) versus the normalized broadening at (a) 263 K and (b) 283 K. The solid straight lines are the HSE component of the dispersion amplitude and the dashed lines the theoretical DD component computed from eq 16 with $2b = 0.38$ at 263 K and $2b = 0.81$ at 288 K. The error bars are one-half the difference in the results computed from the low- and high-field dispersion amplitudes, respectively; i.e., these are a measure of the systematic errors in obtaining the dispersion amplitude. The results from five spectra are plotted separately to indicate the reproducibility.

Table 4. Experimental Values of *b*

T, K	$\Omega(T)$	$2b$
253	0 ± 0.05	0.21 ± 0.06
263	0.09 ± 0.03	0.38 ± 0.04
273	0.27 ± 0.03	0.66 ± 0.07
283	0.51 ± 0.04	0.81 ± 0.14
293	0.77 ± 0.03	1.6 ± 0.30
303	0.90 ± 0.06	2.1 ± 1.2

On the basis of less extensive data, we showed in part 6 that values of (V^{dip}_{disp}/V_{pp}) were well approximated by the following empirical equation:

$$\left[\frac{V^{dip}_{disp}}{V_{pp}}\right] = \left[\frac{V^{dip}_{disp}}{V_{pp}}\right](\infty)\tanh(c/c^*) \tag{34}$$

where the constant $(V^{dip}_{disp}/V_{pp})(\infty)$ is the plateau value at large c and c^* is a characteristic concentration at which the plateau is approached. In this work, with an abundance of points, we are able show in greater detail that eq 34 describes the data within experimental uncertainty for 253−303 K for all values of c. This is described in the Supporting Information. There is no theoretical basis for eq 31; however, may use it to determine accurate relative values of the FITTING constants that are

dx.doi.org/10.1021/jp210057x | J. Phys. Chem. A 2012, 116, 2855−2866

presented in Table S1 of the Supporting Information. From those data, we may conclude that $c^* = 27 \pm 2$ mM for all $T \leq 303$ K . The break points in Figure 8 and at other temperatures, correspond to a common critical concentration of 29 ± 8 mM, where the uncertainty is the estimated error; thus, the intersections of the straight lines in Figure 8 are within experimental uncertainty of c^*. Clearly, the break point occurs at different values of $\langle B\rangle/A_0$. If a FITTING artifact were responsible for the nonlinearity yielding the break points, one expects that the break points would occur at similar line shapes; i.e., similar values of $\langle B\rangle/A_0$. That this is not observed argues for a true effect correlated to the concentration.

The onset of DD can be best observed in a fractional broadening versus T/η plot, Figure 9a. In order to assess the onset of DD we fit the experimental data to the empirical equation $\Omega(T) = [c_1(T/\eta)^2 + c_2(T/\eta) + c_3]/[(T/\eta)^2 + c_4(T/\eta) + c_5]$, and assume that DD becomes significant and clearly observable at $\Omega = 0.95$ (Figure 9a). In the case of pDT in squalane, DD starts at $T/\eta = 24$ K/cP, which corresponds to $\eta = 13.4$ cP at 317 K, while in the case of pDT in 70 wt % glycerol DD starts at $T/\eta = 76$ K/cP, which corresponds to $\eta = 4.4$ cP at 337 K. Using the same method as in the case of the fractional broadening versus T/η plot, we can find the rotational correlation rate $1/\tau_R$ at the onset of DD ($\Omega = 0.95$) (Figure 9b). The rotational rate of pDT at the onset of DD is about 4 times faster in squalane (161 ns^{-1}) than in 70% AG (40 ns^{-1}). Also, it is obvious that the fractional broadening Ω is a smooth function of T/η in the whole region, so the break in the fractional broadening of pDT in water and in 70%AG, Figure 8 of ref 2, is due to solvent effects.

DIFFUSION OF PDT IN ALKANES

Figure 14 shows a comparison between the results in the three alkanes studied in ref 17 and squalane in the region of T/η pertinent to squalane showing that they are rather similar. Nevertheless, there are differences outside of experimental uncertainties. To present a brief comparison, we compare the results at the common value $T/\eta = 135$ K/cP. Extrapolating and interpolating the results to the common value yields $d\langle B_{ex}\rangle/dc = 166$, 142, and 122 G/M in squalane, hexadecane, and decane, respectively. This is a linear variation of $d\langle B_{ex}\rangle/dc$ as a function of the size ratio $\mu = 0.70$, 0.85, and, 1.0, $\mu \equiv r_0/r_{solvent}$, where $r_{solvent}$ is the radius of the solvent, for squalane, hexadecane, and decane, respectively, with $r > 0.999$. Thus, the diffusion coefficient of pDT increases by 36% from squalane to decane, while the hydrodynamic component, computed with eq 21b of ref 17, *decreases* by 16%. Therefore, the short-range component of the diffusion coefficient increases in going from decane to squalane by approximately 50%. Such an increase is expected as discussed in ref 17 due to the increase in free volume. Physically, holes provide a short-range diffusion mechanism independent of the viscosity. Further discussion is beyond the scope of this paper but will appear in a full account together with re-encounter frequencies of pDT in squalane and other solvents as well as other probes in various solvents.

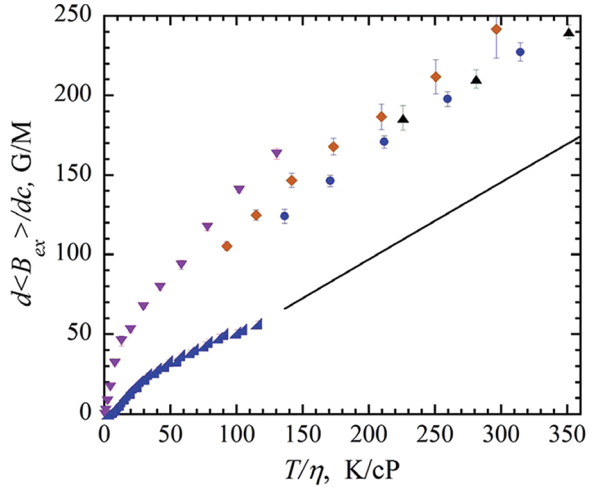

Figure 14. Exchange broadening constant of PDT versus T/η for hexane (▲), decane (●), hexadecane (◆),[17] squalane (▼) and 70% AG (right triangle).[2] The solid line is the SES prediction for pDT (eq 12 of ref 28).

In order to understand the diffusion of a small solute in the progressively larger solvent molecules, Kowert at al. have measured the translational diffusion constant, D, of dioxygen in *n*-alkanes (C7−C16) at room temperature.[30,31] The authors found that the deviations of D from the SE equation increased as the difference in size between solute and solvent increased. When D is plotted as a function of μ, the data can be FITTED to a straight line with a negative slope and a correlation factor of 0.996. If the values of $d\langle B_{ex}\rangle/dc = 32$, 105, 227, and 476 G/M at 293 K in squalane, hexadecane, decane, and hexane, respectively, are plotted as a function of μ, the data also can be well fitted to a negatively sloped line. Therefore, it is very likely that the observed faster diffusion of pDT in squalane is due to the relative size difference between the pDT and squalane molecules.

CONCLUSIONS

The EPR spectral parameters that can be extracted from the EPR spectrum by nonlinear least-squares fitting have been related to the rate constants due to the HSE and DD interactions. The derived relations allow us to successfully separate the two interactions. The fractional broadening $\Omega = \langle B_{ex}\rangle/\langle B\rangle$can be easily calculated from the slope k of a line in a graph of V_{disp}/V_{pp} versus $\langle B\rangle/A_0$, assuming one knows the ratio $b = |V_{dd}|/|W_{dd}|$, which can be calculated for a given molecular diffusion model. The analysis of the simulated data indicates that when the value of W_{dd} becomes about or more than 3% of the value of K_{ex} that the slow motion limit of b can be used without introducing any measurable error. The slope k can also be measured from a graph of A_{abs}/A_0 versus $\langle B\rangle/A_0$, which is demonstrated on the simulated data but is less promising for experimental data due to an interplay of the linear and quadratic terms in eq 28. The DD broadening constant can then be extracted from the broadening constants once Ω is known. The negative values of V_{disp}/V_{pp} and the observed line shifts away from the center of the spectrum at low temperatures are caused by DD and can be fully explained by eqs 1 proposed by Salikhov.[4] The rate constant of encounter collisions of pDT in squalane as a function of T/η is larger than the hydrodynamic prediction and larger than in 70 wt % glycerol (70%AG). The fractional broadening Ω is a continuous function of either τ_R^{-1} or T/η. Ω as a function of T/η is larger in squalane than in 70%AG; however, as a function of rotational rate of pDT, the opposite is observed; i.e., Ω is larger in 70 % AG than in squalane. The differences in the encounter collision rate constants and Ω in a series of alkanes can be explained by the relative size difference between pDT and solvent molecules. In the case of pDT in squalane, DD starts at $T/\eta = 24$ K/cP,

dx.doi.org/10.1021/jp210057x | J. Phys. Chem. A 2012, 116, 2855−2866

which corresponds to η = 13.4 cP at 317 K, while in the case of pDT in 70%AG DD starts at T/η = 76 K/cP, which corresponds to η = 4.4 cP at 337 K. This difference may be due to the relative size difference between the spin probe and solvent molecules.

■ ASSOCIATED CONTENT

Supporting Information

Simulations of eqs 1, correction of $V_{disp}(M_j)/V_{pp}(M_j)$, derivation of eqs 11−14, and analysis of the dispersion signal offset. This information is available free of charge via the Internet at http://pubs.acs.org.

■ AUTHOR INFORMATION

Corresponding Author

*E-mail: peric@usc.edu.

Notes

The authors declare no competing financial interest.

■ ACKNOWLEDGMENTS

M.P. gratefully acknowledges support from NIH Grant S06 GM48680.

■ REFERENCES

(1) Berner, B.; Kivelson, D. *J. Phys. Chem.* **1979**, *83*, 1406−1412.
(2) Bales, B. L.; Meyer, M.; Smith, S.; Peric, M. *J. Phys. Chem. A* **2009**, *113*, 4930−4940.
(3) Galeev, R. T.; Salikhov, K. M. *Chem. Phys. Rep.* **1996**, *15*, 359−375.
(4) Salikhov, K. M. *Appl. Magn. Reson.* **2010**, *38*, 237−256.
(5) Abragam, A. *Principles of Nuclear Magnetism*; Oxford University Press: Oxford, 1986.
(6) Closs, G. L.; Forbes, M. D. E.; Norris, J. R. *J. Phys. Chem.* **1987**, *91*, 3592−3599.
(7) Shushin, A. I. *Chem. Phys. Lett.* **1997**, *275*, 137−144.
(8) Shushin, A. I. *Chem. Phys. Lett.* **1998**, *282*, 413−420.
(9) Tarasov, V. F.; Forbes, M. D. E. *Spectrochim. Acta A* **2000**, *56*, 245−263.
(10) Plachy, W.; Kivelson, D. *J. Chem. Phys.* **1967**, *47*, 3312.
(11) Molin, Y. N.; Salikhov, K. M.; Zamaraev, K. I. *Spin Exchange Principles and Applications in Chemistry and Biology*; Springer: Berlin, 1980.
(12) Salikhov, K. M. *J. Magn. Reson.* **1985**, *63*, 271−279.
(13) Bales, B. L.; Peric, M.; Dragutan, I. *J. Phys. Chem. A* **2003**, *107*, 9086−9098.
(14) Eastman, M. P.; Kooser, R. G.; Das, M. R.; Freed, J. H. *J. Chem. Phys.* **1969**, *51*, 2690−2709.
(15) Eastman, M. P.; Bruno, G. V.; Freed, J. H. *J. Chem. Phys.* **1970**, *52*, 2511−2522.
(16) Bales, B. L.; Peric, M. *J. Phys. Chem. B* **1997**, *101*, 8707−8716.
(17) Kurban, M. R.; Peric, M.; Bales, B. L. *J. Chem. Phys.* **2008**, *129*, 064501−064510.
(18) Bales, B. L.; Peric, M. *J. Phys. Chem. A* **2002**, *106*, 4846−4854.
(19) Bales, B. L.; Meyer, M.; Smith, S.; Peric, M. *J. Phys. Chem. A* **2008**, *112*, 2177−2181.
(20) Bales, B. L. In *Spin Labeling: Theory and Applications*; Berliner, J. L., Reuben, J., Eds.; Plenum: New York, 1989; Vol. *8*, pp 77−130.
(21) Deegan, R. D.; Leheny, R. L.; Menon, N.; Nagel, S. R.; Venerus, D. C. *J. Phys. Chem. B* **1999**, *103*, 4066−4070.
(22) Pensado, A. S.; Comunas, M. J. P.; Lugo, L.; Fernandez, J. *Ind. Eng. Chem. Res.* **2006**, *45*, 2394−2404.
(23) Sax, K. J.; Stross, F. H. *Anal. Chem.* **1957**, *29*, 1700−1702.
(24) Dubey, G. P.; Sharma, M. *Int. J. Thermophys.* **2008**, *29*, 1361−1375.
(25) Barlow, A. J.; Erginsav, A. *Proc. R. Soc. London, Ser. A* **1972**, *327*, 175−190.
(26) Plachy, W. Z.; Windrem, D. A. *J. Magn. Reson.* **1977**, *27*, 237−239.
(27) Alves, M.; Peric, M. *Biophys. Chem.* **2006**, *122*, 66−73.
(28) Bales, B. L.; Harris, F. L.; Peric, M.; Peric, M. *J. Phys. Chem. A* **2009**, *113*, 9295−9303.
(29) Zhao, Y. H.; Abraham, M. H.; Zissimos, A. M. *J. Org. Chem.* **2003**, *68*, 7368−7373.
(30) Kowert, B. A.; Dang, N. C. *J. Phys. Chem. A* **1999**, *103*, 779−781.
(31) Kowert, B. A.; Dang, N. C.; Reed, J. P.; Sobush, K. T.; Seel, L. G. III *J. Phys. Chem. A* **2000**, *104*, 8823−8828.